Journal of Alloys and Compounds 516 (2012) 53–57

Contents lists available at SciVerse ScienceDirect

Journal of Alloys and Compounds

journal homepage: www.elsevier.com/locate/jallcom

Phase structure and electrochemical properties of $La_{0.7}Ce_{0.3}Ni_{3.75}Mn_{0.35}Al_{0.15}Cu_{0.75-x}(Fe_{0.43}B_{0.57})_x$ hydrogen storage alloys

Baozhong Liu[a,*], Mengjuan Hu[a], Liqiang Ji[b], Yanpin Fan[a], Yongguang Wang[b], Zhi Zhang[a], Anming Li[a]

[a] School of Materials Science & Engineering, Henan Polytechnic University, Jiaozuo 454000, China
[b] Inner Mongolia Rare Earth Ovonic Metal Hydride Co. Ltd., Baotou 014030, China

ARTICLE INFO

Article history:
Received 14 October 2011
Received in revised form
23 November 2011
Accepted 24 November 2011
Available online 2 December 2011

Keywords:
Hydrogen storage alloy
FeB alloy
Phase structure
Electrochemical property
Ni/MH batteries

ABSTRACT

Microstructure and electrochemical characteristics of $La_{0.7}Ce_{0.3}Ni_{3.75}Mn_{0.35}Al_{0.15}Cu_{0.75-x}(Fe_{0.43}B_{0.57})_x$ hydrogen storage alloys have been investigated. XRD indicates that $La_{0.7}Ce_{0.3}Ni_{3.75}Mn_{0.35}Al_{0.15}Cu_{0.75}$ alloy consists of a single $LaNi_5$ phase with $CaCu_5$ structure. The alloys containing FeB are composed of $LaNi_5$ phase with $CaCu_5$ structure as matrix phase and $La_3Ni_{13}B_2$ phase as secondary phases, and the abundance of the secondary phase gradually increases with increasing FeB content. As x increases from 0.00 to 0.20, maximum discharge capacity of the alloy electrodes monotonically decreases from 314.0 to 290.4 mAh/g. Cycling stability of the alloy electrodes increases with increasing x value. High-rate dischargeability at the discharge current density of 1200 mA/g first increases from 51.4% (x = 0) to 57.2% (x = 0.10), and then decreases to 52.7% (x = 0.20). The improvement in electrochemical characteristics is ascribed to the secondary phase $La_3Ni_{13}B_2$, which improves the electrochemical activity of electrode surface, as well as to the phase boundary in multiphase structure, which decreases the lattice distortion and strain energy and enhances the anti-pulverization property of the alloy electrodes.

1. Introduction

AB_5-type hydrogen storage alloys are widely used as the negative electrode materials in commercial nickel/metal hydride (Ni/MH) rechargeable batteries by virtue of their advantages, such as good activation ability, high capacity, high resistance to over-charging and over-discharging, capable of performing a high rate charge/discharge, long cycle life and environmental friendliness, etc. [1–3]. However, in recent years, Ni/MH batteries have been confronted with the rapid development of high-power devices, rapidly developing towards the lower cost and the high performance. Especially, the high-rate dischargeability (HRD) is a critical criterion of evaluating properties of hydrogen storage alloys used as negative electrode materials of high-power batteries. Thus, it is very imperative to further lower the cost and improve the HRD of AB_5-type hydrogen storage alloys.

Multi-component alloying is effective to tailor electrochemical performances of hydrogen storage alloys. To decrease the cost of AB_5-type hydrogen storage alloys, it seems greatly significant to investigate the substitution of cheap Fe for expensive Ni or Co. Wei et al. [4] have pointed out that cycle stability of $LaNi_{4.05-x}Al_{0.45}Mn_{0.5}Fe_x$ ($0 \le x \le 0.5$) alloy electrodes increased with the increase of Fe content, but maximum discharge capacity of the alloy electrodes decreased from 334.8 (x = 0) to 292.8 mAh/g (x = 0.5). Vivet et al. [5] have studied electrochemical hydrogen storage properties of $MmNi_{4.07}Mn_{0.63}Al_{0.2}Co_{0.4-x}Fe_x$ ($0 \le x \le 0.4$) alloys and found that Fe-containing electrodes behaved as well as Co-containing electrodes in terms of cycle life with a slight capacity reduction. Zhao et al. [6] observed that cycling stability of $Mm(NiMnSiAl)_{4.3}Co_{0.6-x}Fe_x$ (x = 0–0.6) alloy electrodes increased with increasing x value, but maximum discharge capacity and high-rate dischargeability decreased. Yang et al. [7] have investigated that cycling stability of $LaNi_{3.55}Mn_{0.35}Co_{0.20}Al_{0.20}Cu_{0.85-x}Fe_x$ alloy electrodes enhanced significantly from 77.6% (x = 0.10) to 89.9% (x = 0.60), but the maximum discharge capacity and high-rate dischargeability decreased. Obviously, cycling stability of the alloy electrodes can be improved by the substitution of Ni, Co or Cu by Fe with the decrease of the other electrochemical properties. Furthermore, some work focuses on improving the HRD of AB_5-type hydrogen storage alloys by introducing B in the alloy. Zhang et al. [8] have investigated low Co AB_5-type $MmNi_{3.8}Co_{0.4}Mn_{0.6}Al_{0.2}B_x$ alloys composed of $CaCu_5$-type main phase and a small amount of $CeCo_4B$-type secondary phase and pointed out that the addition of B improved cycling stability and activation performance, high rate discharge capability. The substitution of B for Ni in $MmNi_{3.70-x}Mn_{0.35}Co_{0.60}Al_{0.25}B_x$ alloys has been studied and found that the alloys with B had $LaNi_5$ phase and the secondary phase with $CeCo_4B$-type structure, which improved the activation ability

* Corresponding author. Tel.: +86 391 3989859; fax: +86 391 3989859.
E-mail addresses: bzliu@hpu.edu.cn, b_z_liu@163.com (B. Liu).

0925-8388/$ – see front matter © 2011 Elsevier B.V. All rights reserved.
doi:10.1016/j.jallcom.2011.11.122

and the HRD of alloy electrodes [9]. Ye et al. [10] have reported that $Mm_{3.55}Co_{0.75}Mn_{0.4}Al_{0.3}B_{0.3}$ alloy containing a principal $CaCu_5$-type phase and a small amount of $CeCo_4B$-type secondary phase had good activation performance and high-rate dischargeability. The addition of B in the alloys has been proved to be effective to enhance the activation performance and markedly improve the high-rate dischargeability.

It is inferred that cheap Fe is effective to improve the cycling stability, and B is effective to improve the high-rate dischargeability of hydrogen storage alloys. Moreover, the new La–Fe–B alloys with multiphase structures including $LaNi_5$, $La_3Ni_{13}B_2$ and (Fe, Ni) phases exhibited good activation characteristics, high-rate dischargeability and low-temperature dischargeability [11]. Therefore, it is possible that the combined substitution of Fe and B for Cu in AB_5-type hydrogen storage alloys can improve discharge capacity, high-rate dischargeability and cycling stability. Fortunately, commercial FeB alloy has more advantages than the pure Fe and B, such as cheaper cost and lower melt point, etc. Thus, $La_{0.7}Ce_{0.3}Ni_{3.75}Mn_{0.35}Al_{0.15}Cu_{0.75-x}(Fe_{0.43}B_{0.57})_x$ alloys are chosen as objects. And correspondingly, phase structure, electrochemical properties and kinetics performances of $La_{0.7}Ce_{0.3}Ni_{3.75}Mn_{0.35}Al_{0.15}Cu_{0.75-x}(Fe_{0.43}B_{0.57})_x$ alloys as well as the relationship among them are investigated.

2. Experimental procedures

$La_{0.7}Ce_{0.3}Ni_{3.75}Mn_{0.35}Al_{0.15}Cu_{0.75-x}(Fe_{0.43}B_{0.57})_x$ (x = 0–0.20)alloys were synthesized by induction melting of the metal elements (La, Ce, Ni, Mn, Al, Cu: 99.9% in purity and commercial FeB alloy contains 57.0% B and the other is Fe and trace impurities) under argon atmosphere and then annealed at 1223 K for 10 h.

The phases of the alloy powders were determined by X-ray diffraction (XRD) using a Rigaku D/max 2500PC powder diffractometer with Cu Kα radiation. The phase structures of alloys were analyzed using Jade-5 software.

All the alloy electrodes for test were prepared by cold pressing the mixture of 0.15 g alloy powders of 200–400 meshes and 0.75 g nickel carbonyl powders into a pellet of 10 mm in diameter under 15 MPa, investigated by an electrochemical charging/discharging method. Electrochemical measurements were performed at 298 K in a standard tri-electrode system, consisting of a working electrode (metal hydride), a counter electrode ($Ni(OH)_2$/NiOOH), and a reference electrode (Hg/HgO) with 6 mol/L KOH solution as electrolyte. Each electrode was charged for 7 h at 60 mA/g and discharged to −0.6 V vs. Hg/HgO at 60 mA/g at 298 K. After every charging/discharging, the rest time was 10 min. In evaluating the high-rate dischargeability, discharge capacity of the alloy electrode at different discharge current density was measured. The high-rate dischargeability HRD (%) was defined as $C_d/C_{max} \times 100\%$, where C_d is the discharge capacity at the discharge current density I_d (I_d = 60, 300, 600, 900 and1200 mA/g) and C_{max} is the maximum discharge capacity at the discharge current density I = 60 mA/g.

The electrochemical impedance spectrum (EIS), the linear polarization curve and potential-step measurement were obtained by on PARSTAT 2273, respectively. At 50% depth of discharge (DOD), the electrochemical impedance spectrum (EIS) was tested in the frequency range of 100 kHz to 10 mHz. Linear polarization curves were obtained by scanning the electrodes from −8 to 8 mV (vs. open circuit potential). For potential-step measurement, the electrodes in fully charged state were discharged with potential steps of 0.5 V for 3600 s.

3. Results and discussion

3.1. Crystal structure

Fig. 1 presents XRD patterns of $La_{0.7}Ce_{0.3}Ni_{3.75}Mn_{0.35}Al_{0.15}Cu_{0.75-x}(Fe_{0.43}B_{0.57})_x$ alloys. It can be seen that $La_{0.7}Ce_{0.3}Ni_{3.75}Mn_{0.35}Al_{0.15}Cu_{0.75}$ alloy has a single $CaCu_5$-type $LaNi_5$ phase, and the alloys containing FeB consist of two phases, the matrix phase $LaNi_5$ and the secondary phase $La_3Ni_{13}B_2$. The abundance of $La_3Ni_{13}B_2$ phase increases with the increase of x value. The calculated lattices parameters of $LaNi_5$ phase in all alloys are listed in Table 1. The calculated lattice constant c and c/a ratio of $LaNi_5$ phase increases with the increase of x value.

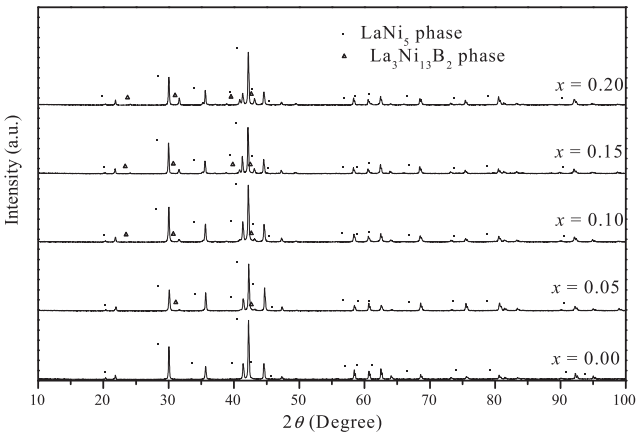

Fig. 1. XRD patterns of $La_{0.7}Ce_{0.3}Ni_{3.75}Mn_{0.35}Al_{0.15}Cu_{0.75-x}(Fe_{0.43}B_{0.57})_x$ alloys.

Table 1
Lattice parameters of $La_{0.7}Ce_{0.3}Ni_{3.75}Mn_{0.35}Al_{0.15}Cu_{0.75-x}(Fe_{0.43}B_{0.57})_x$ alloys.

x	a (Å)	c (Å)	V (Å^3)	c/a
0	5.0269	4.0489	88.6070	0.8054
0.05	5.0290	4.0510	88.7271	0.8055
0.10	5.0291	4.0544	88.8051	0.8062
0.15	5.0253	4.0590	88.7715	0.8077
0.20	5.0208	4.0635	88.7108	0.8093

3.2. Activation capability and discharge capability

The number of cycles (N_a) needed to activate the electrodes and maximum discharge capacity (C_{max}) of $La_{0.7}Ce_{0.3}Ni_{3.75}Mn_{0.35}Al_{0.15}Cu_{0.75-x}(Fe_{0.43}B_{0.57})_x$ alloy electrodes are given in Table 2. It is noted that the alloys containing FeB are easily activated to reach the maximum capacity within 2–3 cycles, but the alloy without FeB needs 4 cycles. It indicates that the substitution of FeB for Cu improves the activation performance of the alloy electrode. Generally, the activation performance of the alloy electrode is related to surface characteristics and phase structure of the alloy [12]. Due to the low surface energy of Fe, the oxidation of Fe on the alloy surface forms easily. The oxidation film becomes thick with the increase of x value, which is unfavorable to activation property. Fortunately, the formation of the secondary phase increases the number of phase boundaries, which provides extra tunnels for the diffusion of hydrogen atoms and is buffer area of the releasing of the stress formed in the process of hydrogen absorbed [8,13]. The increase of $La_3Ni_{13}B_2$ secondary phase causes the increase in the phase boundary, which can decrease the lattice distortion and strain energy formed in the process of hydrogen absorption. Therefore, the improvement of activation performances is mainly attributed to the $La_3Ni_{13}B_2$ secondary phase in the alloys. The C_{max} of alloy electrodes monotonically decreases from 314.0 mAh/g (x = 0) to 290.4 mAh/g (x = 0.20). Generally speaking, C_{max} is related to the phase structure and electrochemical kinetics. The effects of the secondary phase

Table 2
Electrochemical properties of $La_{0.7}Ce_{0.3}Ni_{3.75}Mn_{0.35}Al_{0.15}Cu_{0.75-x}(Fe_{0.43}B_{0.57})_x$ alloys.

x	C_{max} (mAh/g)	N_a [b]	HRD_{1200} [a] (%)	S_{100} (%)
0	314.0	4	51.4	76.4
0.05	308.7	3	54.8	77.8
0.10	301.5	2	57.2	79.5
0.15	296.2	2	53.1	80.4
0.20	290.4	2	52.7	81.6

[a] The high-rate dischargeability at the discharge current density of 1200 mA/g.
[b] The number of cycles needed to activate the electrode.

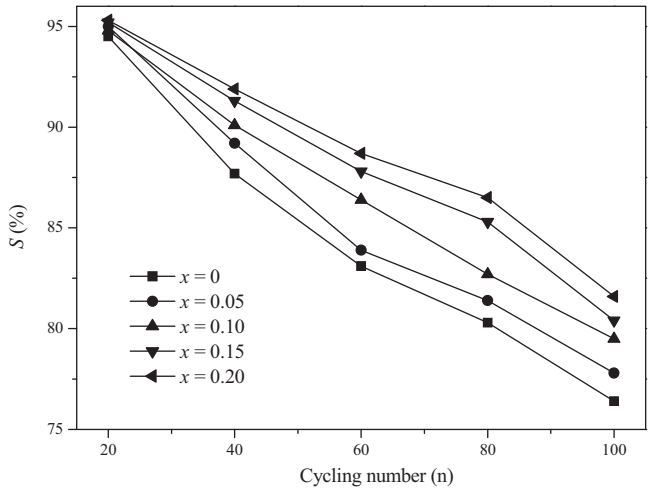

Fig. 2. Cycling stability of $La_{0.7}Ce_{0.3}Ni_{3.75}Mn_{0.35}Al_{0.15}Cu_{0.75-x}(Fe_{0.43}B_{0.57})_x$ alloy electrodes.

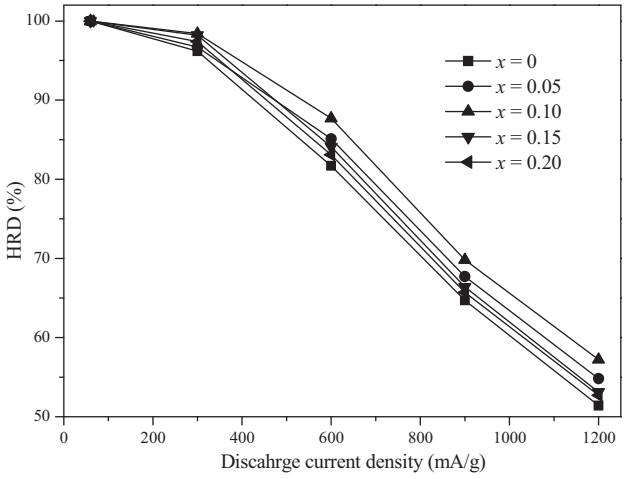

Fig. 3. HRD of $La_{0.7}Ce_{0.3}Ni_{3.75}Mn_{0.35}Al_{0.15}Cu_{0.75-x}(Fe_{0.43}B_{0.57})_x$ alloy electrodes.

$La_3Ni_{13}B_2$ on the discharge capacity of the alloy electrodes are complicated: as mentioned above, the phase boundary of the secondary phase $La_3Ni_{13}B_2$ increasing hydrogen diffusion in the alloys is favorable for the discharge capability, but the hydrogen storage capacity of $La_3Ni_{13}B_2$ phase is 157 mAh/g, which has much lower discharge capacity than the matrix phase $LaNi_5$, which is unfavorable for discharge capability. On the other hand, the increase of Fe content results in the increase of surface oxide film, which will degrade the charge-transfer reaction on the alloy surface. Moreover, the surface oxide film decreases the activity site on the alloy surface, and then makes the hydrogen diffuse from the inner of alloy to the surface more difficult. The increase of surface oxide film resulted from the increase of Fe is also unfavorable the discharge capacity. Thus, it is reasonable that the unfavorable factors are prominent for the decrease of the C_{max} of $La_{0.7}Ce_{0.3}Ni_{3.75}Mn_{0.35}Al_{0.15}Cu_{0.75-x}(Fe_{0.43}B_{0.57})_x$ alloy electrodes.

3.3. Cycling stability

The cycle stability is an extremely important factor for the service life of a hydrogen storage alloy. The discharge capacity of the alloy electrode as a function of cycle number is shown in Fig. 2. The cycling capacity retention rate, expressed as S_n (%) = $C_n/C_{max} \times 100$ (where C_n is the discharge capacity at the nth cycle), is listed in Table 1. It can be seen that S_{100} increases from 76.4% (x = 0) to 81.6% (x = 0.20). It is confirmed that the fundamental reasons for the capacity decay of the electrode alloy are the pulverization of the alloy during charge–discharge cycle [14]. As is well-known that pulverization of AB_5-type metal hydrides during absorption/desorption of hydrogen is an inherent problem that is resulted from the combination of volume change and their brittle nature. The increase in c/a ratio of main-phase facilitates hydrogen atoms from going in and out of the crystal and therefore decreases lattice stress during charging/discharging cycles [15]. The c/a ratio of $LaNi_5$ phase increases with increasing x value, which contributes to lower lattice stress and stronger pulverization resistance. Furthermore, as mentioned above, the secondary phase $La_3Ni_{13}B_2$ increases the amount of phase boundary, which releases the stress formed in the process of hydrogen absorbing and then improves cycling stability. Thus, the substitution of FeB for Cu can improve the cycling stability of the alloy electrodes.

3.4. High-rate dischargeability and electrochemical kinetics

Fig. 3 shows the relationship between the high-rate dischargeability (HRD) and the discharge current density of $La_{0.7}Ce_{0.3}Ni_{3.75}Mn_{0.35}Al_{0.15}Cu_{0.75-x}(Fe_{0.43}B_{0.57})_x$ alloy electrodes. The HRD of the alloy electrodes first increases with increasing x from 0 to 0.10, and then decreases when x increases to 0.20. The HRD at the discharge current density of 1200 mA/g is listed in Table 2. It can be seen that HRD_{1200} first increases from 51.4% (x = 0) to 57.2% (x = 0.10), and then decreases to 52.7% (x = 0.20).

It is well known that the HRD of the MH electrodes is dominated by the electrochemical kinetics of the charge-transfer reaction at the electrode/electrolyte interface and the hydrogen diffusion rate within the bulky alloy electrode, which are reflected in the value of the charge-transfer resistance (R_{ct}) and/or surface exchange current density (I_0), being a measure of the catalytic activity of an alloy, as well as in the hydrogen diffusion coefficient (D), which characterizes the mass transport properties of an alloy electrode [16].

The charge-transfer resistance at the surface of the alloys is determined by the electrochemical impedance spectrum (EIS). Fig. 4 shows the typical electrochemical impedance spectra (EIS) of $La_{0.7}Ce_{0.3}Ni_{3.75}Mn_{0.35}Al_{0.15}Cu_{0.75-x}(Fe_{0.43}B_{0.57})_x$ alloy electrodes at 50% DOD and 298 K. It can be seen that, for all alloy electrodes, each EIS consists of two semicircles at the high-frequency region and a straight line followed by the two semicircles at the low-frequency region. The smaller semicircle in the EIS curve represents the contact resistance between the alloy powder and the conductive material. The larger semicircle in the low-frequency region in

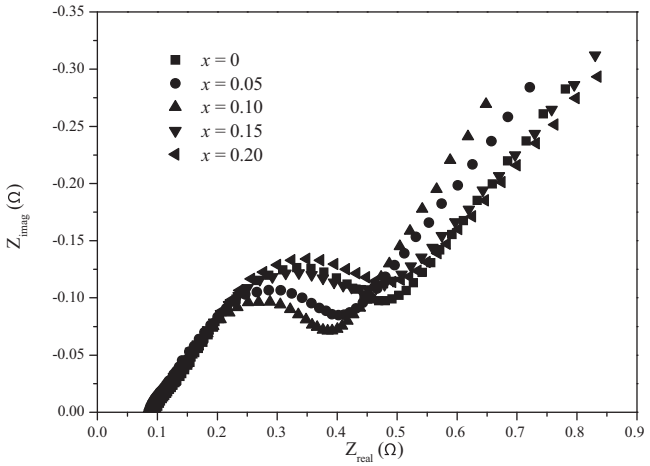

Fig. 4. EIS of $La_{0.7}Ce_{0.3}Ni_{3.75}Mn_{0.35}Al_{0.15}Cu_{0.75-x}(Fe_{0.43}B_{0.57})_x$ alloy electrodes at 50% DOD.

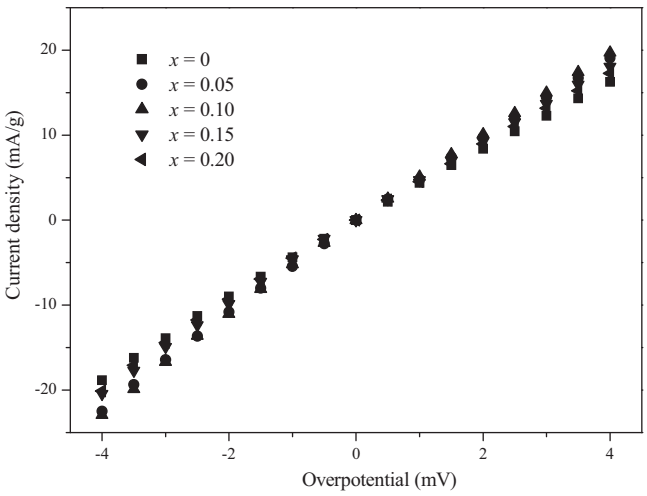

Fig. 5. Linear polarization curves of $La_{0.7}Ce_{0.3}Ni_{3.75}Mn_{0.35}Al_{0.15}Cu_{0.75-x}(Fe_{0.43}B_{0.57})_x$ alloy electrodes at 50% DOD.

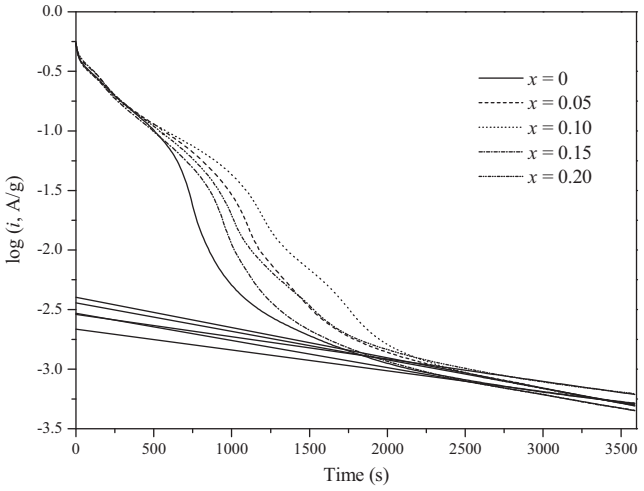

Fig. 6. Semi-logarithmic plots of the anodic current vs. the time response of $La_{0.7}Ce_{0.3}Ni_{3.75}Mn_{0.35}Al_{0.15}Cu_{0.75-x}(Fe_{0.43}B_{0.57})_x$ alloy electrodes.

the spectrum can be characterized as the reaction resistance in the charge-transfer process [17]. As shown in Fig. 4, the radius of the larger semicircle in the low-frequency region first decreases and then increases with increasing x value, and the radius of the larger semicircle is the smallest when x value is 0.10.

Fig. 5 shows the linear polarization curves of $La_{0.7}Ce_{0.3}Ni_{3.75}Mn_{0.35}Al_{0.15}Cu_{0.75-x}(Fe_{0.43}B_{0.57})_x$ alloy electrodes at 50% DOD and 298 K. The polarization resistances R_p are calculated through estimating the slopes of linear polarization curves, and listed in Table 3. The R_p values of the alloy electrodes first decreases from 228.5 ($x=0$) to 188.2 mΩ g ($x=0.10$), and then increases to 216.5 mΩ g ($x=0.20$), which implies that the R_p first decreases and then increases with the increase of FeB content. Besides, the exchange current density I_0 can also describe the charge-transfer process. The I_0 value can be calculated according to the following formula [18].

$$I_0 = \frac{RT}{FR_p} \tag{1}$$

where R, T, F, R_p are the gas constant, the absolute temperature, the Faraday constant and the polarization resistance, respectively. The I_0 are calculated by Eq. (1) listed in Table 3. It is clear that the I_0 first increases from 112.4 ($x=0$) to 136.4 mA/g ($x=0.10$), and then decreases to 118.6 mA/g ($x=0.20$). It is reported that the formation of the secondary phase improves the catalytic activity of the alloys [10,11]. As mentioned above, the secondary phase $La_3Ni_{13}B_2$ increases with increasing x value, which is beneficial to the electrocatalytic activity of the surface of alloy electrode and improves the charge-transfer reaction. On the other hand, Increasing Fe will cause the increase of surface oxide film and then degrade the charge-transfer reaction on the alloy surface. Therefore, it is reasonable to assume that, when $x \leq 0.10$, the favorable effect is chiefly responsible for the increase of the exchange current density for alloy electrodes. However, when $x > 0.10$, the decrease of the exchange current density for alloy electrodes is mainly ascribed to the disadvantageous factors. It is believed that the change of the exchange current density for alloy electrodes with increasing x value should be attributed to the combined effect of advantageous and disadvantageous factors.

Table 3
Electrochemical kinetic characteristics of $La_{0.7}Ce_{0.3}Ni_{3.75}Mn_{0.35}Al_{0.15}Cu_{0.75-x}(Fe_{0.43}B_{0.57})_x$ alloy electrodes.

x	R_p (mΩ g)	I_0 (mA/g)	D ($\times 10^{-11}$ cm^2/s)
0	228.5	112.4	6.89
0.05	195.3	131.5	9.04
0.10	188.2	136.4	10.0
0.15	208.4	123.2	7.99
0.20	216.5	118.6	7.40

The diffusion coefficient of hydrogen in the alloy electrodes is determined with the potential-step method. Fig. 6 shows the semi-logarithmic plots of the anodic current vs. the time response of the $La_{0.7}Ce_{0.3}Ni_{3.75}Mn_{0.35}Al_{0.15}Cu_{0.75-x}(Fe_{0.43}B_{0.57})_x$ alloy electrodes. Zheng et al. [19] have reported that MH electrode reaction would be controlled by the rate of hydrogen diffusion in the bulk of alloys, when the rate of charge-transfer on the surface of alloy electrodes was so fast that the hydrogen concentration nearly equal to zero under a large anodic potential-step. Assuming that the grains of alloys are all spherical, and the initial hydrogen concentration in the bulk of the alloy is uniform and the hydrogen surface concentration is constant. When the discharge time is long enough, the hydrogen diffusion coefficient D can be calculated by the slope from the linear plot of $\log(i)$ vs. t using the following formula.

$$\log i = \log\left(\frac{6FD}{da^2}(C_0 - C_s)\right) - \frac{\pi^2}{2.303}\frac{D}{a^2}t \tag{2}$$

where i is anodic current density (A/g), D the hydrogen diffusion coefficient (cm^2/s), d the density of the alloy (g/cm^3), a the radius of the alloy particle, C_0 the initial hydrogen concentration in the bulk of the alloy (mol/cm^3), C_s the surface hydrogen concentration of the alloy (mol/cm^3) and t is the discharge time (s). The particle size is measured by Malvern particle analyzer Mastersizer 2000 and the average particle radius is about 13 μm. D calculated according to the formula above is summarized in Table 3. The D of $La_{0.7}Ce_{0.3}Ni_{3.75}Mn_{0.35}Al_{0.15}Cu_{0.75-x}(Fe_{0.43}B_{0.57})_x$ alloy electrodes first increases from 6.89×10^{-11} ($x=0$) to 10.0×10^{-11} cm^2/s ($x=0.10$), and then decreases to 7.40×10^{-11} cm^2/s ($x=0.20$). As mentioned above, the phase boundary of the secondary phase $La_3Ni_{13}B_2$ increasing is favorable for hydrogen diffusion. Moreover, it is also claimed that the stability of metal hydride gradually decreases with increasing B content x [9]. The increase of B content, induced by FeB alloy additive, will lower the stability of the alloy hydride and then cause the hydrogen desorption easily, which contributed to hydrogen diffusion. On the other hand, Iwakura et al. [20] have reported that the oxidation of Fe on the alloy surface limited the hydrogen transfer from the surface to the bulk of the alloys, which is detrimental to the hydrogen diffusion. As mentioned above, the increase of Fe content causes the increase

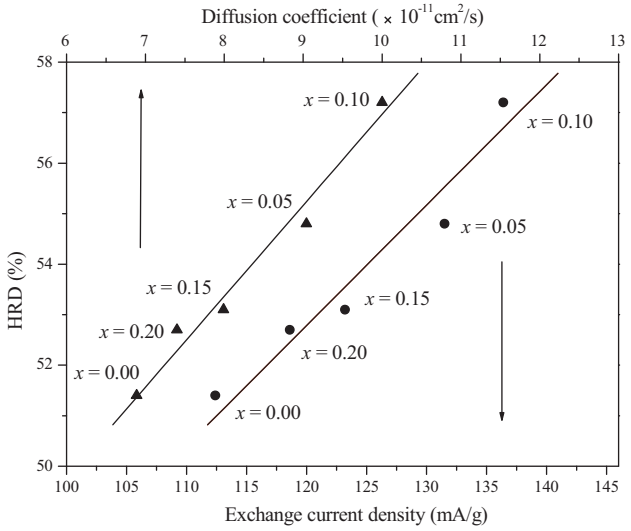

Fig. 7. High-rate discharge (HRD_{1200}) as a function of excharge current density I_0 and hydrogen diffusion coefficient for $La_{0.7}Ce_{0.3}Ni_{3.75}Mn_{0.35}Al_{0.15}Cu_{0.75-x}(Fe_{0.43}B_{0.57})_x$ alloy electrodes.

of surface oxide film, which will degrade the hydrogen diffusion. Thus, it is considered that both advantageous and disadvantageous factors work on the change of the hydrogen diffusion of the alloy electrodes.

Iwakura et al. [21,22] have reported that if the electrochemical kinetics at the electrode/electrolyte interface was rate-determining, a linear dependence of the high-rate dischargeability on the exchange current density should be observed. In contrast, if the diffusion of hydrogen in the alloy was rate-determining, a linear dependence of the high-rate dischargeability on the hydrogen diffusion coefficient should be found. Fig. 7 shows the HRD_{1200} as a function of the I_0 and the D of $La_{0.7}Ce_{0.3}Ni_{3.75}Mn_{0.35}Al_{0.15}Cu_{0.75-x}(Fe_{0.43}B_{0.57})_x$ alloy electrodes. It is evident that the HRD_{1200} increases with the increase of the I_0 and the D, and shows a linear relationship with the I_0 and the D, respectively. This implies that both charge-transfer reaction at the electrode/electrolyte interface and the hydrogen diffusion of alloy electrodes should be responsible for the HRD at a discharge current density of 1200 mA/g.

4. Conclusions

$La_{0.7}Ce_{0.3}Ni_{3.75}Mn_{0.35}Al_{0.15}Cu_{0.75}$ alloy has a single $CaCu_5$-type $LaNi_5$ phase, and the alloys containing FeB consist of two phases, the matrix phase $LaNi_5$ and the secondary phase $La_3Ni_{13}B_2$. The amount of $La_3Ni_{13}B_2$ phase increases with the increase of x value. As the content of FeB increases, maximum discharge capacity decreases from 314.0 to 290.4 mAh/g. S_{100} increases from 76.4% ($x = 0$) to 81.6% ($x = 0.20$). The improvement in cycle stability should be ascribed to the increase of c/a and the formation of the secondary phase, which improves the anti-pulverization property. The HRD of alloy electrodes, exchange current density I_0 and hydrogen diffusion coefficient D first increases and then decreases with the increase of FeB content and the alloy with $x = 0.10$ has the highest value. Both charge-transfer reaction at the electrode/electrolyte interface and the hydrogen diffusion of alloy electrodes should be responsible for the high-rate dischargeability.

Acknowledgements

This research is financially supported by the National Natural Science Foundation of China (51001043), and China Postdoctoral Science Foundation funded project (20100470990), and the Doctoral Foundation of Henan Polytechnical University (B2010-13).

References

[1] S.R. Ovshinsky, M.A. Fetcenko, J. Ross, Science 260 (1993) 176–181.
[2] T. Sakai, I. Uehara, H. Ishikawa, J. Alloys Compd. 293–295 (1999) 762–769.
[3] F. Feng, M. Geng, D.O. Northwood, Int. J. Hydrogen Energy 26 (2001) 725–734.
[4] X.D. Wei, S.S. Liu, H. Dong, P. Zhang, Y.N. Liu, J.W. Zhu, G. Yu, Electrochim. Acta 52 (2007) 2423–2428.
[5] S. Vivet, J.M. Joubert, B. Knosp, A. Percheron-Guégan, J. Alloys Compd. 356–357 (2003) 779–783.
[6] Y.P. Zhao, Y.H. Zhang, G.Q. Wang, X.P. Dong, S.H. Guo, X.L. Wang, J. Alloys Compd. 388 (2005) 284–292.
[7] S.X. Yang, Y. Li, Z.P. Liu, S.Q. Yang, S.M. Han, Acta Phys.-Chim. Sin. 26 (2010) 2144–2150.
[8] Y.H. Zhang, M.Y. Chen, X.L. Wang, G.Q. Wang, X.P. Dong, Y. Qi, Electrochim. Acta 49 (2004) 1161–1168.
[9] S.Q. Yang, S.M. Han, Y. Li, S.X. Yang, L. Hu, Mater. Sci. Eng. B 176 (2010) 231–237.
[10] H. Ye, Y.X. Huang, J.X. Chen, H. Zhang, J. Power Sources 103 (2002) 293–299.
[11] H.Z. Yan, F.Q. Kong, W. Xiong, B.Q. Li, J. Li, L. Wang, Int. J. Hydrogen Energy 35 (2010) 5687–5692.
[12] Y. Zhou, Y.Q. Lei, Y.C. Luo, S.A. Cheng, Q.D. Wang, Acta Metall. Sin. 32 (1996) 857–861.
[13] P. Li, X.L. Wang, Y.H. Zhang, R. Li, J.M. Wu, X.H. Qu, J. Alloys Compd. 353 (2003) 278–282.
[14] D. Chartouni, F. Meli, A. Zuttel, K. Gross, L. Schlapbach, J. Alloys Compd. 241 (1996) 160–166.
[15] M. Takao, S. Satoshi, S. Naofumi, European Patent 1,075,032, A1 (2001).
[16] H.G. Pan, J.X. Ma, C.S. Wang, S.A. Chen, X.H. Wang, C.P. Chen, Q.D. Wang, J. Alloys Compd. 293–295 (1999) 648–652.
[17] N. Kuriyama, T. Sakai, H. Miyamura, I. Uehara, H. Ishikawa, T. Iwasaki, J. Alloys Compd. 202 (1993) 183–197.
[18] P.H.L. Notten, P. Hokkeling, J. Electrochem. Soc. 138 (1991) 1877–1885.
[19] G. Zheng, B.N. Popov, R.E. White, J. Electrochem. Soc. 142 (1995) 2695–2698.
[20] C. Khaldi, H. Mathlouthi, J. Lamloumi, A. Percheron-Guégan, J. Alloys Compd. 360 (2003) 266–271.
[21] C. Iwakura, T. Oura, H. Inoue, M. Matsuoka, Electrochim. Acta 41 (1996) 117–181.
[22] C. Iwakura, M. Miyamoto, H. Inoue, M. Matsuoka, Y. Fukumoto, J. Alloys Compd. 259 (1997) 132–134.